

## ROTATION OF GIANT STARS

YEVGENI KISSIN

Department of Astronomy and Astrophysics, University of Toronto, 50 St. George St., Toronto, ON M5S 3H4, Canada

CHRISTOPHER THOMPSON

Canadian Institute for Theoretical Astrophysics, 60 St. George St., Toronto, ON M5H 3H8, Canada

*Draft version August 5, 2021*

### ABSTRACT

The internal rotation of post-main sequence stars is investigated, in response to the convective pumping of angular momentum toward the stellar core, combined with a tight magnetic coupling between core and envelope. The spin evolution is calculated using model stars of initial mass 1, 1.5 and  $5 M_{\odot}$ , taking into account mass loss on the giant branches. We also include the deposition of orbital angular momentum from a sub-stellar companion, as influenced by tidal drag along with the excitation of orbital eccentricity by a fluctuating gravitational quadrupole moment. A range of angular velocity profiles  $\Omega(r)$  is considered in the envelope, extending from solid rotation to constant specific angular momentum. We focus on the backreaction of the Coriolis force, and the threshold for dynamo action in the inner envelope. Quantitative agreement with measurements of core rotation in subgiants and post-He core flash stars by *Kepler* is obtained with a two-layer angular velocity profile: uniform specific angular momentum where the Coriolis parameter  $\text{Co} \equiv \Omega\tau_{\text{con}} \lesssim 1$  (here  $\tau_{\text{con}}$  is the convective time); and  $\Omega(r) \propto r^{-1}$  where  $\text{Co} \gtrsim 1$ . The inner profile is interpreted in terms of a balance between the Coriolis force and angular pressure gradients driven by radially extended convective plumes. Inward angular momentum pumping reduces the surface rotation of subgiants, and the need for a rejuvenated magnetic wind torque. The co-evolution of internal magnetic fields and rotation is considered in Kissin & Thompson, along with the breaking of the rotational coupling between core and envelope due to heavy mass loss.

*Subject headings:* stars: giants – stars: white dwarfs – stars: rotation – magnetic fields

### 1. INTRODUCTION

Measurements of internal oscillation modes of red giant stars by the *Kepler* satellite have been used to infer rapid rotation in the radiative core – in some cases, an order of magnitude faster than at the surface (Beck et al. 2012; Mosser et al. 2012). This evidence has been interpreted by Cantiello et al. (2014) in terms of a decoupling of the rotation of the core from the convective envelope, which is assumed to rotate as a solid body.

Here we reconsider the role that convection plays in redistributing angular momentum within a star. So far only a limited understanding has been developed of the interaction between rotation and convection. The most convincing theoretical calculations involve direct numerical simulations (e.g. Brun & Palacios 2009).

Red giants offer a promising test case, because (i) the influence of the Coriolis force is reduced (although not entirely eliminated) in comparison with main sequence (MS) stars; (ii) the great depth of the convective envelope reduces the effect of boundary conditions on the angular velocity profile; and (iii) feedback from magnetic fields on the rotation profile is less important, especially near the tip of the red giant and asymptotic giant branches (RGB and AGB), where most of the envelope rotates slowly. Disentangling the most important processes that control the rotation profile of a star is, for these reasons, easier in red giants than in the Sun.

The internal rotation of giant stars also has important implications for the magnetism and spin of their white dwarf (WD) remnants. A basic theme of this paper, and

the companion paper (Kissin & Thompson 2015, hereafter Paper II) is that one must consider the co-evolution of rotation and magnetic fields if one is to understand either. The strong flow of material from the hydrogen-rich envelope, through burning shell(s), and into the core implies that one cannot treat core and envelope in isolation from each other.

This observation leads us to discard models of the rotation which neglect the influence of large-scale poloidal magnetic fields that were deposited by previous convective activity. For example, the Modules for Experiments in Stellar Astrophysics (MESA) code (Paxton et al. 2011) implements a heuristic prescription for angular momentum redistribution in the radiative parts of a star, which starts with the current-driven (Taylor) instability of a predominantly toroidal magnetic field, leading to a poloidal component that is then wound back by differential rotation into the toroidal direction (Spruit 2002).

The nearly solid rotation of the Sun's core has been used to infer the presence of a helical magnetic field (Gough & McIntyre 1998). The introduction of a persistent twist to the field not only facilitates hydromagnetic stability (Braithwaite & Spruit 2004), but also suppresses differential rotation across poloidal magnetic flux surfaces. The minimal poloidal field that will transport angular momentum rapidly enough to compensate changes in the core mass profile on the MS is only  $\sim 10^{-6}$  G; but a field  $\sim 10^2$ - $10^3$  times stronger is required to compensate a latitude-dependent convective stress that is partly transmitted through a tachocline layer into the

core (Paper II). The ascent of the early red giant branch is completed over a Gyr, not a great deal shorter than the present age of the Sun, meaning that a similarly weak poloidal magnetic flux would enforce nearly solid rotation in the core of a subgiant (e.g. Maeder & Meynet 2014).

In a  $1-2M_{\odot}$  star, the source of this field differs between the early and later stages of post-MS expansion. The envelope expands in mass during the first dredge-up phase, so that any remnant field in the outer core would have been deposited by a vigorously convective and rapidly rotating envelope during the pre-MS contraction, when magnetic fields several orders of magnitude stronger were present. The minimal poloidal magnetic field that pushes the core toward solid rotation is well below the threshold of detectability if transported to the surface of the star. We note that our assumption of solid rotation in radiative material depends on the relative weakness of additional processes that might source differential rotation, such as the damping of gravity waves that are excited in adjacent convective zones.

We are led to a simpler model for the angular momentum profile in a post-MS star: nearly solid rotation in the core, as enforced by large-scale Maxwell stresses, combined with inhomogeneous rotation in the convective envelope. The details of a dynamo operating around the core-envelope boundary, the ensuing flow of magnetic helicity into the core, and the conditions under which the dynamo shuts off and core and envelope decouple, are addressed in Paper II. Here our focus is on the angular velocity profile of the envelope, especially as it is influenced by the Coriolis force.

Convective Reynolds stresses appear to transport angular momentum inward in accretion flows (Balbus et al. 1996). This effect is demonstrated in stars with extended convective envelopes by Brun & Palacios (2009) using three-dimensional anelastic simulations. In slowly rotating cases, most relevant to the present discussion, the specific angular momentum is found to be independent of radius.

The rotation frequency of the solar convective envelope is, by contrast, roughly independent of radius – a fact that appears to have influenced treatments of rotation in the post-MS phase. Although the solar envelope also covers many scale heights, it has a modest aspect ratio (0.7:1 in radius), implying that thermal boundary conditions have a stronger influence on the rotation profile than in a star with a deep envelope (e.g. Browning et al. 2006). The Sun is not especially rapidly rotating by the standards of late-type MS stars, although the Coriolis force still has a significant effect on its rotation profile. The rotation period  $P_{\text{rot}} = 2\pi/\Omega$  is about 3 times the local convective time  $\tau_{\text{con}} = \ell_P/v_{\text{con}}$  (where  $v_{\text{con}}$  is the speed of a convective eddy and  $\ell_P$  the pressure scale height), corresponding to a Coriolis parameter  $\text{Co} \equiv \Omega\tau_{\text{con}} \sim 2$ . Dynamo action may also influence the rotation profile (Brun et al. 2004).

The most important decision to be made here is how to handle the backreaction of the Coriolis force on the inward pumping of angular momentum. We investigate two simple prescriptions: i) a balance between the Coriolis force and non-radial pressure gradient forces that result from the entropy difference between convective downflows and upflows; and ii) an upper limit  $\text{Co} \sim 1$  in the inner envelope, representing an approximate balance

between the Coriolis and inertial forces. Both of these prescriptions are compared against asteroseismic fits to *Kepler* data for subgiants and post-core He flash stars. We find that prescription i) provides a very promising quantitative fit.

Measurements of surface rotation in subgiants provide independent constraints on the internal angular momentum distribution in post-MS stars. Schrijver & Pols (1993) have used stellar models to argue for an inconsistency between these surface measurements and the evolution of  $\sim 1.5 M_{\odot}$  subgiants that maintain solid rotation. Adding a more rapidly rotating core, while maintaining solid rotation in the envelope, was found to have a negligible impact on the result. The discrepancy between models and data was therefore interpreted in terms of an additional magnetic wind torque acting on a star as it develops a convective envelope upon leaving the MS.

Here we show that the same inward pumping of angular momentum in the envelope that reproduces the *Kepler* observations also causes a factor  $\sim 1/2$  reduction in surface rotation speed over the same interval, thereby removing most (but not necessarily all) of the evidence for a magnetic wind torque. The calculations presented here, and in Paper II, neglect any rotational effect of surface magnetic fields during the post-MS phase.

We also extend our considerations to the tip of the RGB and AGB. Here the Coriolis force has a reduced effect, due to the greater expansion of the star ( $\gtrsim 10$  times larger than the *Kepler* sample analyzed by Beck et al. 2012 and Mosser et al. 2012). This leads us to consider more inwardly peaked rotation profiles than the one suggested by fitting *Kepler* data.

A final consideration is binary interaction. This is especially important for stars which lose most of their natal angular momentum to a magnetized wind on the MS, corresponding to an initial mass  $\lesssim 1.3 M_{\odot}$ . After such a star ascends to the upper RGB or AGB, the inward pumping of angular momentum cannot, by itself, sustain  $\text{Co} \gtrsim 1$  in the convective envelope.

A robust hydromagnetic dynamo is maintained during the greatest expansion of the star only if it encounters an external source of angular momentum. We consider the interaction of a convecting giant with a companion planet, calculating the combined orbital evolution of the planet and the change in the angular momentum of the star. An interesting detail of this evolution is the excitation of orbital eccentricity by the gravitational quadrupole associated with large-scale convective eddies in the giant. In the case of a planetary companion, this effect is much more pronounced than when the companion is a neutron star (Phinney 1992), and we show that it extends the range of orbital periods within which the planet gives up its orbital angular momentum to the star.

### 1.1. Plan of the Paper

We investigate the rotation profile of a deep convective envelope in Section 2, with a focus on the backreaction of the Coriolis force on angular momentum pumping. Various angular velocity profiles are compared against the *Kepler* measurements of core rotation for subgiants and post-He flash stars in Section 3. The effect of angular momentum pumping on the evolution of surface rotation of subgiants is examined in Section 3.2.

In Section 4, we consider the rotational evolution of

model stars of initial mass 1 and  $5 M_\odot$ , including the effects of convective pumping, angular momentum loss to a wind, and planetary interaction. Details of the evolution of the orbit of a planet around an expanding giant are given in Section 5, including drag from the tide raised on the star and the excitation of eccentricity by a convective quadrupole.

Some outstanding questions are addressed in the concluding Section 6. The appendix gives further details of our calculation of eccentricity growth in the orbit of a companion planet.

## 2. PUMPING OF ANGULAR MOMENTUM IN DEEP CONVECTIVE ENVELOPES: BACKREACTION FROM THE CORIOLIS FORCE

The deep convective envelope of a giant star divides into an outer part that is slowly rotating ( $\text{Co} \lesssim 1$ ); and an inner part where  $\text{Co} \gtrsim 1$  and the rotation profile is influenced by the Coriolis force.

The entire envelope may rotate slowly near maximum expansion, especially if the spin angular momentum of the star has been strongly depleted by a magnetized wind during the MS phase. On the other hand, a star is still compact enough during the early stages of post-MS expansion that  $\Omega\tau_{\text{con}} \gg 1$  throughout much of the convective envelope.

We imagine that entropy is approximately conserved over downflows and upflows that are extended compared with a local scale height. Some indirect evidence for such a configuration has long been obtained from one-dimensional models of giant convection, which require a mixing length exceeding a single scale height (Sackmann & Boothroyd 1991).

Such a suppression of radial mixing is suggestive of an inwardly peaked rotation profile in the outer, slowly rotating envelope, corresponding to the conservation of specific angular momentum  $j$  by individual convective flows – as indeed is obtained numerically by Brun & Palacios (2009). Rotation profiles intermediate between  $\Omega(r) \propto r^{-2}$  and solid rotation could clearly be obtained from limited mixing, but for definiteness we focus here on the simple case  $\partial j / \partial r \rightarrow 0$  where  $\text{Co} < 1$ . Obtaining the angular velocity profile in the inner envelope depends on a more detailed analysis of the Coriolis force, which we give below.

We consider the evolving partition between fast and slow rotation in Section 3.1, and how it depends on the angular momentum retained (or gained) by the star in Section 4. Given a flat distribution of specific angular momentum in the outer envelope, an intermediate-mass star generally sustains an inner zone where  $\text{Co} \gtrsim 1$ , even near the tip of the RGB or AGB; but a star which spins down on the MS must gain angular momentum from a planetary or stellar companion.

### 2.1. Extended Upflows and Downflows with Quasi-Geostrophic Balance

When the inner zone with  $\text{Co} \gtrsim 1$  covers a wide range of radius, we can look for a power-law scaling of the rotation frequency  $\Omega$  with spherical radius. The stellar envelope is nearly adiabatic and spherically stratified. In this inner zone of fast rotation ( $\Omega r \sin \theta \gg v_{\text{con}}$ ) about an axis  $\hat{z}$  ( $\theta = 0$ ), the steady vorticity equation reads

(e.g. Balbus 2009)

$$r \sin \theta \frac{\partial \Omega^2}{\partial z} \simeq -\frac{1}{C_p \rho r} \frac{\partial P}{\partial r} \frac{\partial S}{\partial \theta} = \frac{g(r)}{C_p r} \frac{\partial S}{\partial \theta}. \quad (1)$$

Here  $P$  and  $\rho$  are pressure and density,  $g(r) = GM(r)/r^2$  is gravity, and the specific entropy is  $S = [\mu(\gamma - 1)]^{-1} \ln(P/\rho^\gamma)$ , approximated here as that of an ideal gas with mean atomic weight  $\mu$  and specific heat  $C_p$  ( $C_v$ ) at constant pressure (volume).

The ‘thermal wind’ approximation used in Equation (1) holds because  $|\partial P / \partial \theta| \ll |\partial P / \partial \ln r|$ . In the upper, slowly rotating part of the envelope, the latitudinal pressure gradient is sourced by the entropy difference between upflows and downflows, and is smaller by a factor  $(v_{\text{con}}/c_s)^2$  than the radial gradient. Our focus here is on a rapidly rotating solution to Equation (1), where the angular pressure gradient which sources  $\partial S / \partial \theta$  is proportional to  $\Omega^2$ .

When the gravitating mass in the inner envelope is dominated by the stellar core, gravity  $g(r) \propto r^{-2}$ . From Equation (1) we obtain the ansatz

$$\Omega^2(r, \theta) = \Omega^2(R_c) \left( \frac{r}{R_c} \right)^{-3} f(\cos \theta). \quad (2)$$

Here  $R_c$  is the radius inside of which  $\text{Co} \gtrsim 1$ .

One subtlety here is that the stellar mass profile is not as centrally concentrated during the early subgiant expansion. This generally leads to a shallower scaling of  $\Omega$  with  $r$ : taking  $g(r) \propto r^{-\beta}$ , with  $\beta < 2$ , we find  $\Omega(r) \propto r^{-(1+\beta)/2}$ . A fit to the gravity profile in the inner convective envelope over the range of expansion that is probed by the *Kepler* asteroseismic data gives  $\beta \sim 1$ , corresponding to  $\Omega(r) \propto r^{-1}$ . The monopolar scaling of  $g$  is approached following the first dredge-up, and is maintained near the tips of the RGB and AGB.

We imagine that the rotation profile organizes at  $\text{Co} \gg 1$  into axially symmetric rolls. In other words, the strong latitudinal dependence of the Coriolis force is hypothesized to translate into a persistent latitudinal entropy gradient. If, furthermore, the entropy is conserved along radially extended convective plumes, then we can decompose the entropy profile into low-order spherical harmonics,  $S(r, \theta, \phi) = S_0 + \delta S_0 P_\ell(\cos \theta)$ . Substituting this into Equation (1) along with Equation (2), and normalizing  $f = 1$  at  $\theta = 0$ , we get

$$f = 1 \quad (\ell = 2); \quad f = \frac{21}{20} \cos^2 \theta - \frac{1}{20} \quad (\ell = 4);$$

$$f = \frac{1}{280} (495 \cos^4 \theta - 234 \cos^2 \theta + 19) \quad (\ell = 6). \quad (3)$$

Angular and radial gradients in  $\Omega$  are generally comparable in this type of flow (excepting the simplest case of a quadrupolar entropy pattern). We note that rotation is fastest at the pole for a given  $\ell$  (corresponding to an ‘anti-solar’ rotation profile), but that the opposing gradient can be obtained by superposing  $\ell = 2$  with any higher harmonic. A small anti-rotation is also present in a narrow latitudinal band when the entropy follows a single spherical harmonic.

A caveat here involves our neglect of the Lorentz force, which may have a considerable influence near the boundary of a convection zone, but does not obviously compete

with the right-hand side of equation (1) within a deep convective layer. In particular, the magnetorotational instability (MRI) is ineffective in the outer part of the envelope where  $\text{Co} < 1$ , because the growth time of a MRI mode is longer than the convective time.

### 2.2. Rapid Mixing Between Upflows and Downflows

We now turn to consider the consequences of rapid mixing between upflows and downflows for the rotation profile in parts of the envelope that reach  $\text{Co} \sim 1$ . This provides a useful comparison with the results of Section 2.1, and demonstrates how the radial angular velocity gradient is tied to the presence of radially extended convective flows. We show that the downward advection of angular momentum cannot push the flow to  $\text{Co} \gg 1$  in the inner part of an extended envelope, where  $\tau_{\text{con}}$  decreases inward. This result has a simple interpretation: the competition between the Coriolis force and the inertial force limits  $\text{Co}$  to a value of the order of unity.

In the mixing length approximation, the entropy difference between upflows and downflows is related to the speed of a convective eddy by (e.g. Bethe 1990)

$$\delta S = \frac{\delta h}{k_{\text{B}}T} = \frac{C_p}{C_p - C_v} \frac{v_{\text{con}}^2}{k_{\text{B}}T}. \quad (4)$$

Here  $\delta h$  is the perturbation to specific enthalpy and  $T$  is temperature. Then the angular entropy gradient can be estimated as  $\partial S/\partial\theta \sim (r/\ell_P)\delta S$ . Because it turns out that  $\text{Co} = O(1)$ , we cannot take Equation (1) literally, but can still use it to estimate the magnitude of the shift of angular velocity across a scale height:

$$\delta(\Omega^2) \sim \frac{g(r)}{\ell_P} \frac{v_{\text{con}}^2 \mu}{k_{\text{B}}T} = \left( \frac{v_{\text{con}}}{\ell_P} \right)^2. \quad (5)$$

We look for a rotation profile that diverges inward, so that the constant term in  $\Omega$  can be neglected. Then we find

$$\Omega(r) \sim \frac{v_{\text{con}}(r)}{\ell_P}. \quad (6)$$

As advertised, the Coriolis parameter does not rise much above unity. (Faster rotation can, of course, still be obtained by superposing uniform rotation on the flow.)

For example, in a nearly adiabatic envelope with  $g(r) \propto r^{-2}$ , the speed of an eddy scales as  $v_{\text{con}} \propto (\rho r^2)^{-1/3}$ . Then  $\rho(r) \propto r^{-3/2}$  implies  $\Omega(r) \propto r^{-7/6}$  for  $\gamma = 5/3$ , which is shallower than the profile (2).

### 2.3. Model $\bar{\Omega}(r)$ Profiles

A simple parameterization of the rotation profile which incorporates these lessons may be constructed as follows. Where the Coriolis force can be neglected, at  $r > R_c$ , we consider a flat distribution of specific angular momentum,

$$\bar{\Omega}(r) = \bar{\Omega}(R_c) \left( \frac{r}{R_c} \right)^{-2}; \quad r > R_c. \quad (7)$$

Here  $\bar{\Omega}$  is the angular velocity averaged over a spherical shell. If the angular momentum of the star is small enough that  $\bar{\Omega}(r)\tau_{\text{con}} < 1$  throughout the envelope, then we identify  $R_c$  with the base of the envelope,

$$R_c = R_{\text{benv}}; \quad (\Omega\tau_{\text{con}} < 1 \text{ at } R_{\text{benv}}). \quad (8)$$

When the star has more angular momentum, we maintain the profile (7) in the outer part of the convection zone, and consider

$$\begin{aligned} \text{(I)} \quad \bar{\Omega}(r) &= \bar{\Omega}(R_c) \left( \frac{r}{R_c} \right)^{-\alpha} \\ &= \frac{\text{Co}_{\text{trans}}}{\tau_{\text{con}}(R_c)} \left( \frac{r}{R_c} \right)^{-\alpha}; \quad R_{\text{benv}} < r < R_c \end{aligned} \quad (9)$$

in the inner envelope. Here  $\text{Co}_{\text{trans}} = O(1)$ . As the angular momentum increases  $R_c$  moves outward, and may reach the outer radius of the star, in which case  $\text{Co}$  is larger than unity everywhere in the envelope.

Following the above discussion, we will explore power-law indices  $1 < \alpha < 3/2$ , with the preferred value depending on the radial scaling of gravity. Such a rotation profile corresponds to transport of energy by radially extended, adiabatic plumes.

A second profile, based on mixing length theory, is obtained by setting  $\text{Co}$  to a constant everywhere inside the radius  $R_c$ ,

$$\text{(II)} \quad \bar{\Omega}(r) = \frac{\text{Co}_{\text{trans}}}{\tau_{\text{con}}(r)} + \Omega_0; \quad R_{\text{benv}} < r < R_c. \quad (10)$$

The most important difference with profile I is that  $\text{Co}$  remains pegged at  $\text{Co}_{\text{trans}} \sim 1$  in the absence of the constant term. Setting  $\Omega_0 = 0$  strictly limits the angular momentum which the envelope may contain, a bound which is easily violated during core helium burning. We also require that  $R_c$  is bounded above by the radius at which  $\tau_{\text{con}}$  reaches a maximum; this prevents the formation of a layer below the photosphere in which  $\bar{\Omega}$  increases outward. See Figure 1.

### 2.4. Latitudinal Differential Rotation

The latitudinal shift in rotation frequency (e.g. between pole and equator) has an important influence on the growth of magnetic helicity in the growing core of an RGB or AGB star (Paper II). In rotation model I, where  $\text{Co} > 1$  is maintained by radially extended convective flows, we deduce a strong latitudinal shift:  $\Delta\Omega/\Omega \equiv (\Omega_{\text{eq}} - \Omega_{\text{pole}})/\Omega \sim 1$ . A strong shift is also maintained in the mixing length approximation (rotation model II), as long as the envelope rotates rapidly enough to maintain  $\text{Co} \sim 1$  at the base of the envelope. It is seen in the more rapidly rotating simulations of Brun & Palacios (2009).

We note that weaker latitudinal differential rotation is expected in a compact convective envelope with  $v_{\text{con}} \ll \Omega r \sin\theta$ , as is encountered in the Sun,  $\Delta\Omega/\Omega \propto \text{Co}^{-2}$ .

### 2.5. Matching of Rotation between Core and Convective Envelope

The rotation of core and envelope are easily coupled to each other when the inner envelope retains enough angular momentum to sustain a large-scale hydromagnetic dynamo. The details of this coupling depend on whether the core grows, or recedes, as measured in the radial mass coordinate. When the core is growing, the instantaneous state of the dynamo is the main consideration, because magnetic fields that are amplified near the core-envelope boundary are advected downward. When the

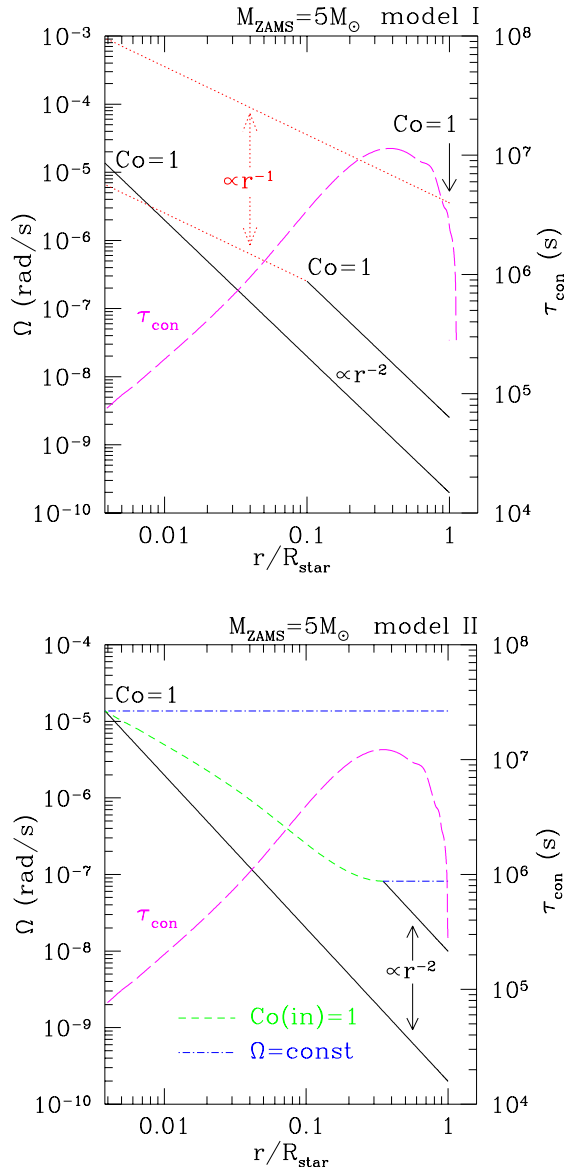


FIG. 1.— Examples of rotation models I (top panel) and II (bottom panel), both taken from the  $5 M_{\odot}$  model near the tip of the AGB. Each panel shows several rotation profiles corresponding to different total stellar angular momenta. The magenta curve shows, for reference, the profile of  $\tau_{\text{con}}(r)$ . Black solid lines represent segments where  $\Omega(r) \propto r^{-2}$  and red dotted lines  $\Omega(r) \propto r^{-1}$ . Top panel: as  $J_{\star}$  is increased, the transition radius  $R_c$ , for which  $\text{Co}(R_c) = 1$ , moves outward. Bottom panel: profiles from bottom to top represent models with increasing  $J_{\star}$ , but now when  $R_c$  reaches the radius of maximum  $\tau_{\text{con}}$ , we begin to add a uniform  $\Omega$  component (the last term in Equation (10)). This prevents the formation of an outer zone of positive  $\partial\Omega/\partial r$ . Black curve: constant  $j$ , reaching  $\text{Co} = 1$  at the base of the envelope; green curve:  $\Omega(r) = v_{\text{con}}/\ell_P$ ; blue curves: constant  $\Omega$  component that grows with increasing  $J_{\star}$ . *Kepler* asteroseismic data favor model I over model II.

core is receding in mass (as it does when a star first ascends the giant branch during the first dredge-up phase), the coupling also depends on a prior dynamo process that implanted a magnetic field in the core material.

A key consideration is the magnitude of the drift speed  $v_r - dR_{\text{benv}}/dt$  of stellar material with respect to the core-envelope boundary (averaged if necessary over ther-

mal pulsations, which are present on the terminal AGB). Solid rotation is enforced in the outer core during downward drift if the radial Alfvén speed is larger than this drift speed. This requires that the large-scale poloidal magnetic field that is generated in the inner envelope be strong enough that

$$\frac{B_r^2}{4\pi\rho(R_{\text{benv}})v_{\text{con}}^2} \gtrsim \frac{(v_r - dR_{\text{benv}}/dt)^2}{v_{\text{con}}^2}. \quad (11)$$

We show in Figure 2 both the drift speed relative to the core-envelope boundary, and the convective speed in the inner envelope (as evaluated using mixing-length theory), during the post-MS evolution of a  $1.5 M_{\odot}$  model star. The same quantities are also shown for a  $5 M_{\odot}$  star near the tip of the AGB. (Further details of these models are described in Sections 3 and 4.)

One sees that during the early subgiant expansion of the  $1.5 M_{\odot}$  model, the remnant poloidal magnetic field in the outer core need only retain an energy density that exceeds  $\sim 10^{-16} - 10^{-15}$  of the instantaneous convective energy density in order to compensate changes in rotation induced by the evolving mass profile. Magnetic fields  $\sim 10^2 - 10^3$  times stronger are needed to compensate a latitude-dependent convective stress (Paper II).

The envelope decreases more rapidly in mass near the tip of the RGB and AGB, and the magnetic energy density that is self-consistently generated during these phases must rise to about  $\sim 10^{-8} - 10^{-6}$  of the convective energy density. We conclude that magnetic decoupling of core from envelope is most easily achieved during the brief phase where the envelope is expelled.

In Section 3 we concentrate on the comparison with *Kepler* asteroseismic data, which only covers post-MS stars more compact than  $\sim 10 R_{\odot}$ . These subgiants and core He burning stars evolve on a relatively long timescale ( $\sim 10^2$  times the duration of the thermally pulsating AGB phase). The results shown in Figure 2 strongly suggest that the rotation of core and envelope remain well coupled in these stars.

We therefore take the core to rotate as a solid with the mean rotation at the base of the envelope,

$$\Omega_{\text{core}} = \Omega_{\text{benv}} \equiv \bar{\Omega}(R_{\text{benv}}). \quad (12)$$

An explanation for the rotation behavior of the *Kepler* sample must be found in the redistribution of angular momentum within an extended convective envelope.

### 3. COMPARISON OF $1.5 M_{\odot}$ MODEL STAR WITH *KEPLER* DATA

We begin by calibrating the rotation models described by Equations (7) and (9)-(12) against the core rotation periods of  $1 - 2 M_{\odot}$  subgiants and post-core He flash stars as measured by Beck et al. (2012) and Mosser et al. (2012). For ease of comparison, we use the same stellar model as Cantiello et al. (2014), namely a  $1.5 M_{\odot}$  star of solar metallicity with zero-age main sequence (ZAMS) equatorial rotation speed  $50 \text{ km s}^{-1}$ .

Our calculation also employs the 1D stellar evolution code MESA (Paxton et al. 2011, version 5527), but with the built-in prescriptions for angular momentum transport turned off. Instead, the rotation profile is ‘patched’ onto the sequence of stellar models.

The total spin angular momentum of the star is evolved

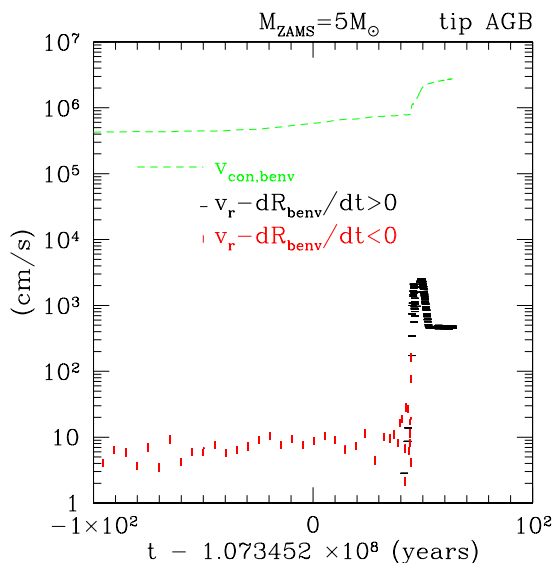
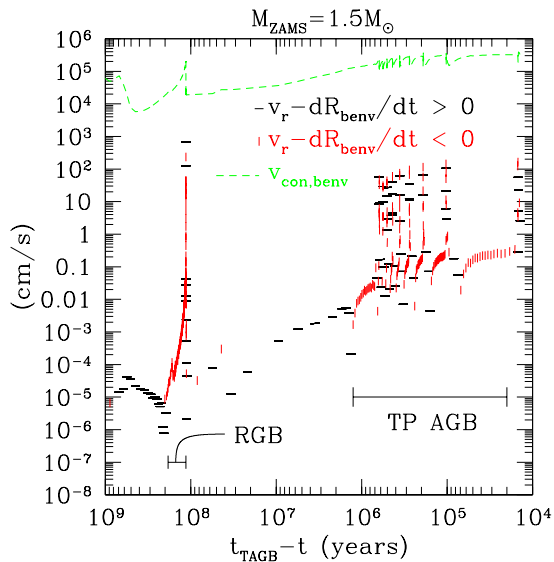


FIG. 2.— Flow speed of stellar material with respect to the core-envelope boundary, compared with convective speed in the inner envelope. Upper panel:  $1.5 M_{\odot}$  model from the early subgiant expansion to the thermally pulsating AGB. Bottom panel:  $5 M_{\odot}$  model at the tip of the AGB. The logarithmic abscissa in the upper panel is referenced to the time  $t_{\text{TAGB}}$  of envelope ejection. The time coordinate in the lower panel has been shifted to focus on the final few hundred years.

self-consistently in response to mass loss, using the prescription described in Section 4.1. Magnetic wind torques are neglected, for the reasons described in Section 3.2. The net effect of mass loss is found to be modest up to the onset of core He burning: a factor  $\sim 2$  reduction in angular momentum during the RGB phase.

We observe from Figure 3 that the inner envelope must rotate rapidly ( $\text{Co}_{\text{benv}} > 1$ ), even in the case of solid rotation, over the range of expansion probed by the *Kepler* data. The rotation period  $P_{\text{benv}} = 2\pi/\Omega_{\text{benv}}$  at the base of the envelope would actually decrease with increasing expansion if the entire envelope could sustain a profile  $\Omega(r) \propto r^{-2}$ .

This effect is still present in the less peaked rotation

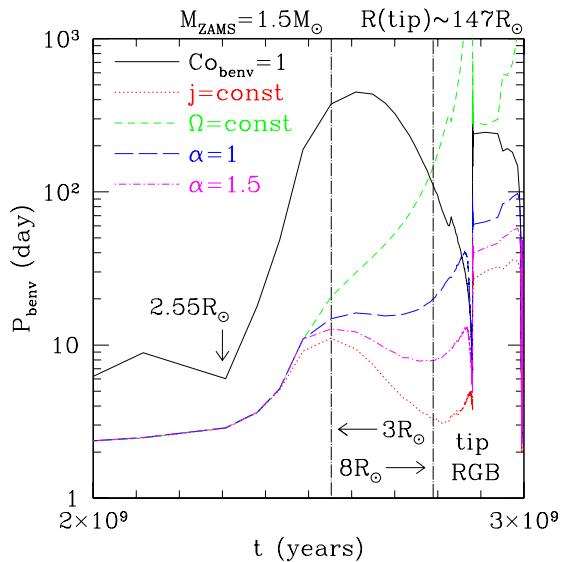


FIG. 3.— Rotation period at the base of the convective envelope, in a  $M_{\text{ZAMS}} = 1.5 M_{\odot}$  model star, as a function of time during the RGB and early core He burning phases. Curves correspond to different rotation profiles. Black line: rotation period  $P_{\text{benv}}$  corresponding to  $\text{Co}_{\text{benv}} = 1$  (with  $\tau_{\text{con}}$  evaluated in the mixing-length approximation). Green dashed line: solid rotation. Red dotted line: uniform specific angular momentum (even where  $\text{Co} > 1$ ). Blue long-dashed line: rotation model I given by Equations (7), (9) with  $\alpha = 1$ . Magenta dashed-dotted line: rotation model I with  $\alpha = 3/2$ . Vertical black lines show the age range probed by the *Kepler* subgiant measurements, with corresponding stellar radius.

profile I, as given by Equations (7), (9) with  $\alpha = 1$  (or  $3/2$ ). Now  $P_{\text{benv}}$  sits close to the observed range of 10–20 days. This period is identified here with the core rotation period.

Another important feature is the large jump in rotation period between the red giant and core He burning phases (Figure 4). The latter, slower, rotation results from a retraction of the convective envelope combined with continuing angular momentum pumping and core-envelope synchronization. (It was previously ascribed by Cantiello et al. (2014) to the conservation of angular momentum by an expanding core that has already decoupled rotationally from the inner envelope.)

A closer look at the effect of the inner rotation index  $\alpha$ , and the initial rotation speed of the star, is provided by Figures 4 and 5. Here one sees that an index  $\alpha$  around 1–1.1 provides a close agreement with the *Kepler* measurements for stars more massive than  $\sim 1.3 M_{\odot}$ . There is some degeneracy between the effects of changing  $\alpha$  and initial rotation speed. It is interesting to note that this profile agrees well with the analytic scaling derived for rotation model I in Section 2.1 in the case (appropriate to the expansion phase probed by the *Kepler* data) where  $g(r) \propto r^{-1}$  in the inner envelope. Recall that this rotation model represents radially extended upflows and downflows in a geometrically deep, adiabatic envelope.

A different conclusion emerges for stars close to solar mass. We see in the bottom panel of Figure 4 that the core of a  $1 M_{\odot}$  star without a close planetary companion is predicted to spin  $\sim 5$ – $10$  times more slowly during subgiant expansion than is seen in our  $1.5 M_{\odot}$  model. On the other hand, the core rotation during the He burning phase is only  $\sim 3$  times slower, and indeed

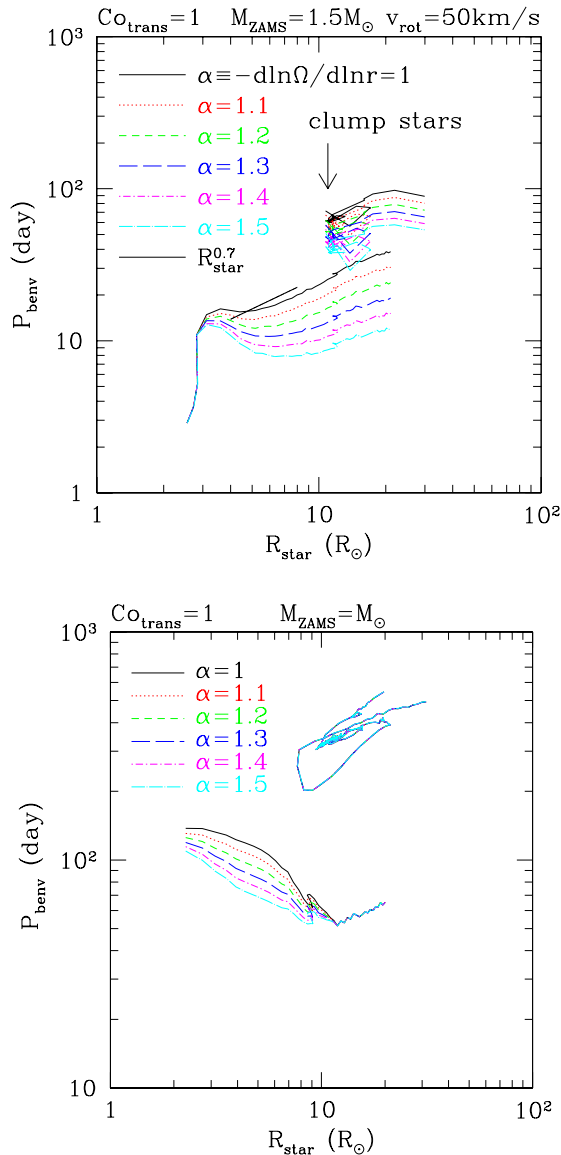


FIG. 4.— Rotation period at the base of the convective envelope during the early giant expansion and the core He burning phase of a  $1.5 M_{\odot}$  star (upper panel) and a  $1 M_{\odot}$  star (lower panel). Rotation model I given by Equations (7), (9) with  $\text{Co}_{\text{trans}} = 1$  and varying inner index  $\alpha$  (here  $\Omega(r) \propto r^{-\alpha}$  inside the radius  $R_c$  where  $\text{Co} = \text{Co}_{\text{trans}}$ ). The  $1.5 M_{\odot}$  star is given a ZAMS equatorial rotation speed  $50 \text{ km s}^{-1}$ , while the  $1 M_{\odot}$  star is given the solar rotational angular momentum. Diagonal black line: fit to *Kepler* subgiant data from Cantiello et al. (2014). The radius at which majority of helium clump stars are found is marked in the upper panel.

remains within the range measured by *Kepler* for clump stars. Significant spindown by magnetic wind torques during the subgiant phase (van Saders & Pinsonneault 2013) would have similar effects.

### 3.1. Transition from $\text{Co} \gtrsim 1$ to $\text{Co} \lesssim 1$ throughout Bulk of Convective Envelope

The *Kepler* sample of subgiants and core He burning stars probes a different rotational regime than is experienced by most giants near their maximum expansion. The *Kepler* stars are compact enough that we find  $\text{Co} \gtrsim 1$  throughout most of the convective envelope, excepting a

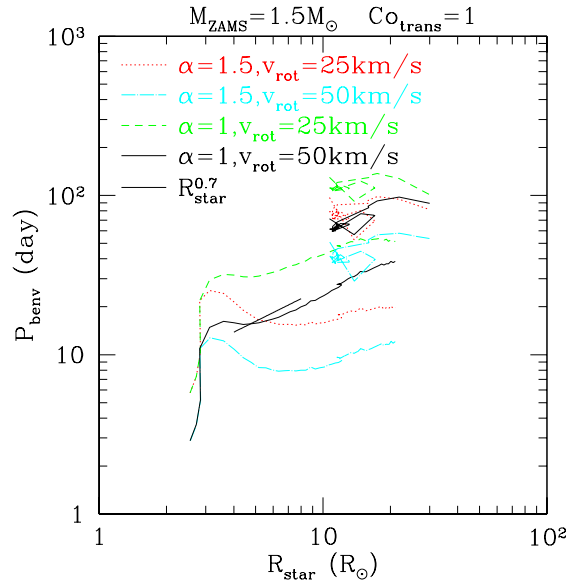


FIG. 5.— Same as upper panel of Figure 4, but now for various initial rotation speeds of the  $1.5 M_{\odot}$  star, and two selected scalings for  $\Omega(r)$  in the rapidly rotating inner zone.

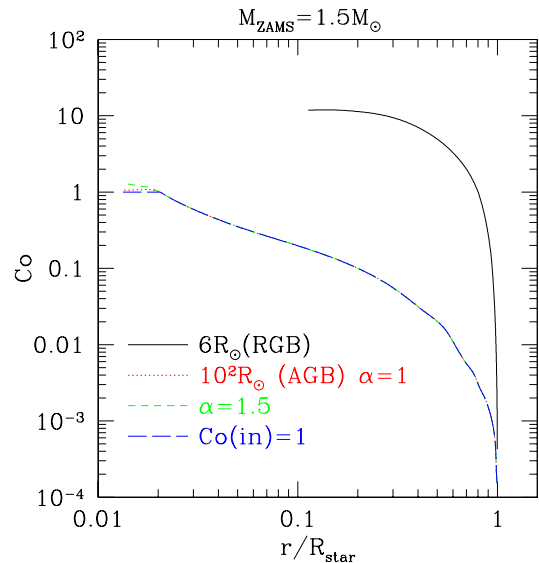


FIG. 6.— Profile of Coriolis parameter with radius during two phases of the evolution of our  $1.5 M_{\odot}$  model with initial  $v_{\text{rot}} = 50 \text{ km s}^{-1}$ . Black curve: subgiant (stellar radius  $6 R_{\odot}$ ) with inner rotation index  $\alpha = 1$  in Equation (9). Colored curves: near the tip of the AGB (stellar radius  $10^2 R_{\odot}$ ) with uniform specific angular momentum in outer envelope, and inner rotation profile corresponding to either  $\alpha = 1$  or  $1.5$ , or to  $\text{Co}$  saturating at unity.

relatively thin layer below the surface. Indeed  $\text{Co}$  reaches a considerable value  $\sim 10 - 30$  at the base of the envelope (Figure 6). The measured core rotation rates probe the angular velocity profile that is sustained in the envelope in a regime of relatively rapid rotation.

Figure 7 shows the evolving partition between an outer zone with uniform specific angular momentum, and an inner zone with angular velocity parameterized by Equation (9). These curves correspond to a star with spin angular momentum close to its birth value, assuming an

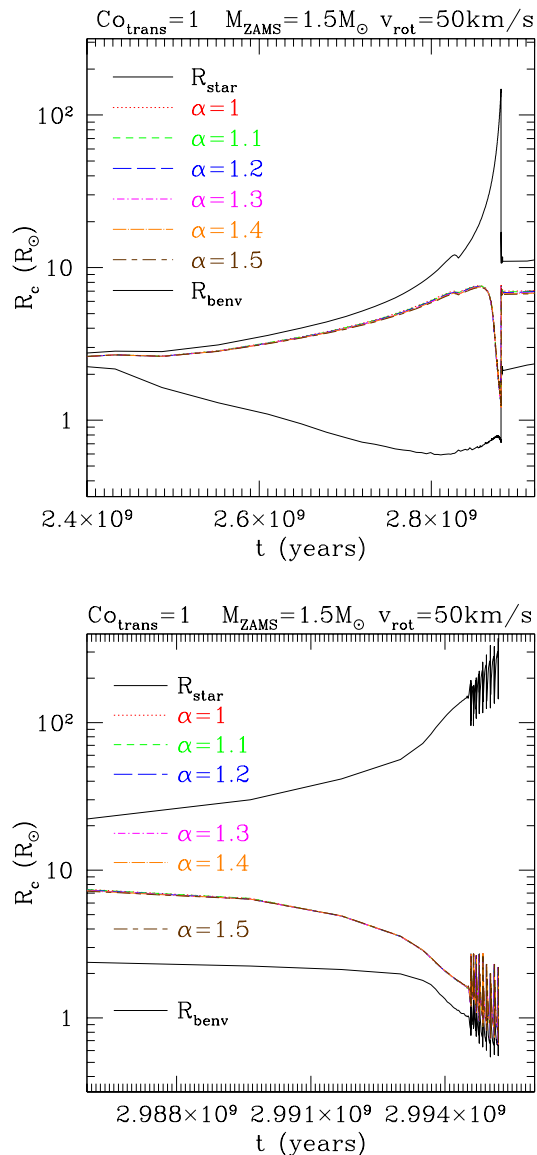


FIG. 7.— Profile of convective envelope during RGB expansion (top panel) and AGB expansion (bottom panel) in rotation model I. As the aspect ratio of stellar radius to the base of the envelope grows, the domain within which  $\text{Co} \gtrsim 1$  shrinks. The radius  $R_c$  marks the transition point between an outer zone with uniform specific angular momentum, and an inner zone with  $\Omega(r) \propto r^{-\alpha}$ . This transition depends only weakly on the inner index  $\alpha$ , because most of the angular momentum is stored in the outer envelope.

equatorial surface rotation speed of  $50 \text{ km s}^{-1}$ . Out to a stellar radius  $R_* \sim 10 R_\odot$ , the envelope remains compact enough that  $\log(R_*/R_c) \lesssim \log(R_c/R_{\text{benv}})$ . Beyond this size, the inner rotation rate is controlled by the rotation profile at  $\text{Co} \lesssim 1$ .

The spin and magnetization of the WD remnant, as explored in Paper II, are strongly influenced by the  $\Omega(r)$  profile of a *slowly* rotating convective envelope near the tip of the RGB and AGB. Then the gravity profile steepens in the inner envelope, and we maintain consideration of rotation profiles at  $\text{Co} > 1$  that are somewhat steeper than suggested by the fit to *Kepler* data:  $\alpha \sim 3/2$  as opposed to  $\alpha \sim 1$  in Equation (9).

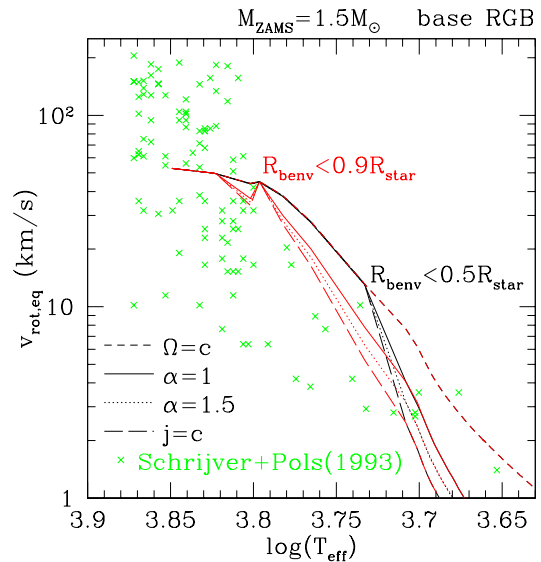


FIG. 8.— Green crosses: observed surface rotation speeds of class IV stars from Schrijver & Pols (1993), multiplied by  $4/\pi$  to account for unknown inclination, as a function of effective temperature. We show for comparison our model of a  $1.5 M_\odot$  star on the early red giant branch, with initial rotation speed  $50 \text{ km s}^{-1}$ . Curves correspond to different profiles of rotation in the envelope, combined with solid rotation in the core. Solid rotation is enforced in the envelope when the aspect ratio  $R_{\text{benv}}/R_*$  between the base of the envelope and stellar photosphere is larger than 0.9 or 0.5. The  $\alpha = 1, 1.5$  curves correspond to rotation model I. In the case  $\alpha = 1$  (which best reproduces the asteroseismic fits to *Kepler* data) there is a factor  $\sim 1/2$  reduction in surface rotation compared with a solid rotator at  $\log(T_{\text{eff}}) < 3.8$ .

### 3.2. Surface Rotation of Subgiants:

#### Angular Momentum Pumping Versus Magnetized Winds

The expansion of a star following the MS phase is associated with a drop in surface rotation. The strength of this drop is sensitive to the distribution of angular momentum within the star, as well as to external torques associated with magnetic activity in the deepening envelope. Schrijver & Pols (1993) and van Saders & Pinsonneault (2013) have presented evidence for an inconsistency between solid rotation in the envelope and measurements in the surface rotation of  $1.5\text{--}2 M_\odot$  stars: the measured rotation is a factor  $\sim 2\text{--}3$  slower than is expected for constant stellar angular momentum.

A similar effect would be imposed by inward pumping of angular momentum. Schrijver & Pols (1993) show that a fast-spinning core has a negligible effect on the result if the convective envelope maintains solid rotation, but did not consider envelopes with inward-peaked rotation profiles. The key point here is that the radiative core becomes very compact early in the expansion onto the red giant branch, in the sense that its moment of inertia is a very small fraction of  $M_{\text{benv}} R_{\text{benv}}^2$ . Therefore inhomogeneous rotation in the envelope has a much larger effect on surface rotation than does a fast-spinning core.

We show in Figure 8 the evolution of the surface rotation in our  $1.5 M_\odot$  model, for the same set of inhomogeneous rotation profiles that we have previously explored. The envelope at high  $T_{\text{eff}}$  is still relatively thin. We therefore impose  $\partial\Omega/\partial r = 0$ , to mimic the solar rota-

tion profile, when the aspect ratio  $R_{\text{benv}}/R_*$  rises above a critical value 0.5 or 0.9. The profile that is favored by the *Kepler* core rotation data, Equations (7) and (9) with inner index  $\alpha = 1$ , shows a factor  $\sim 1/2$  reduction in surface rotation compared with the solid rotator. This removes a significant part of the discrepancy found by Schrijver & Pols (1993) and van Saders & Pinsonneault (2013), but perhaps not all.

#### 4. EVOLVING ROTATION PROFILE WITH MASS LOSS AND INTERACTION WITH A PLANET

We now consider the rotational evolution of a star as it approaches the tip of the RGB and AGB. Here the probability of interacting with a companion increases significantly. The Coriolis parameter also drops markedly at the base of the convective envelope. We maintain our focus on a two-layered rotation model.

Two test cases are analyzed in detail: a star with initial mass  $M_{\text{ZAMS}} = 1 M_\odot$ , which experiences strong spin-down on the MS and interacts with a planet; and an intermediate-mass star ( $M_{\text{ZAMS}} = 5 M_\odot$ ) which remains rapidly rotating at the end of the MS and leaves behind a massive WD. This second stellar model is also allowed to interact with a companion. MESA is used to evolve these stellar models (both of solar metallicity) from the ZAMS to the post-AGB phase.

In the case of the solar-mass star, the interaction with a planet was followed from the base of the RGB, when the star has expanded to a radius  $R_* \sim 10.9 R_\odot$  (age  $t_{10.9} \sim 12.37$  Gyr). At that point, the spin angular momentum was set equal to that of the present Sun. Stellar quantities at times intermediate between the outputted MESA models were obtained by linear interpolation. Details of the orbital integration and the interaction between planet and star are presented in Section 5.

The equatorial rotation speed of the  $5 M_\odot$  star is set to  $50 \text{ km s}^{-1}$  at the ZAMS, corresponding to the peak in the measured  $v \sin i$  distribution (Wolff et al. 2007). Both the  $1 M_\odot$  and  $5 M_\odot$  models are taken to rotate as a solid body on the MS. Deviations from solid body rotation develop after the formation of a deep convective envelope, following the approach of Section 2.

There are instances around the tip of the AGB when the outer envelope splits into several convection zones, separated by radiative layers. The entropy gradient in these radiative zones, although positive, remains small. We impose a matching of specific angular momentum across them.

##### 4.1. Loss of Angular Momentum on the RGB and AGB

Magnetic wind braking is not taken into account in our simulations during the subgiant or giant phases, for the reasons given in Section 3.2. Then the ejected mass carries the specific angular momentum of the stellar photosphere,

$$\dot{J}_* = \frac{2}{3} \bar{\Omega}(R_*) R_*^2 \dot{M}_*. \quad (13)$$

The rate of mass loss on the RGB is handled using the prescription of Reimers (1975),

$$\dot{M}_{* \text{Reimers}} = 4 \times 10^{-13} \eta_R \frac{\tilde{L}_* \tilde{R}_*}{M_*} M_\odot \text{ yr}^{-1}, \quad (14)$$

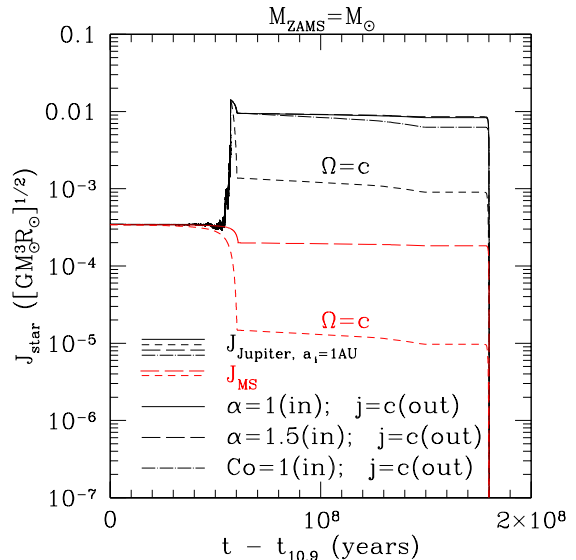


FIG. 9.— Evolution of spin angular momentum of  $1 M_\odot$  model star during RGB, core He burning and final AGB phases. Curves represent cases described in the text. Red lines ( $J_{\text{MS}}$ ): no external source of angular momentum. Black lines ( $J_{\text{Jupiter}, a_i=1\text{AU}}$ ): absorption of a Jupiter-mass planet orbiting initially at  $a_i = 1$  AU. Short dashed lines ( $\Omega = c$ ): solid rotation throughout core and envelope. Other lines correspond to two-layer rotation model, with uniform specific angular momentum in outer envelope, and varying inner rotation profile. Solid (long-dashed) curves:  $\alpha = 1$  ( $\alpha = 1.5$ ) in Equation (9); long-dashed-dotted curve: profile (10) with  $\text{Co} = 1$  in inner zone.

with  $\eta_R = 0.5$ . Here ( $\tilde{\phantom{x}}$ ) denotes stellar parameters measured in solar units. On the AGB we use

$$\dot{M}_{* \text{Bloeker}} = 1.93 \times 10^{-21} \eta_B \frac{\tilde{L}_*^{3.7} \tilde{R}_*}{M_*^{3.1}} M_\odot \text{ yr}^{-1} \quad (15)$$

from Bloeker (1995). Mass loss according to the Bloeker formula is turned on when the central H and He abundances are less than  $10^{-2}$  and  $10^{-4}$ , respectively.

The choice of AGB mass loss parameter  $\eta_B$  is motivated by recent cluster data (e.g. Dobbie et al. 2009). As we discuss further in Paper II, we set  $\eta_B = 0.05$ , corresponding to a final WD mass  $M_{\text{WD}} \sim 0.87 M_\odot$  (from the  $5 M_\odot$  progenitor). The same wind parameters are used for both the  $1 M_\odot$  and  $5 M_\odot$  models. The solar-type star loses  $\sim 0.25 M_\odot$  on the RGB and another  $\sim 0.21 M_\odot$  on the AGB for a final WD mass  $M_{\text{WD}} \sim 0.54 M_\odot$ .

##### 4.2. Rotation Rate of the Inner Envelope and Core

There is a simple relation between spin angular momentum and core angular velocity  $\Omega_{\text{benv}}$  when the envelope is extended and maintains uniform angular momentum per unit mass,

$$j(r) \equiv \frac{dJ(r)}{dM(r)} = \frac{2}{3} r^2 \bar{\Omega}(r) = \text{const.} \quad (16)$$

Given a net stellar angular momentum  $J_*$ , and an effective moment of inertia in the convective envelope,

$$I_{\text{eff}} = \frac{2}{3} \int 4\pi r^2 R_{\text{benv}}^2 \rho(r) dr = \frac{2}{3} R_{\text{benv}}^2 (M_* - M_{\text{benv}}), \quad (17)$$

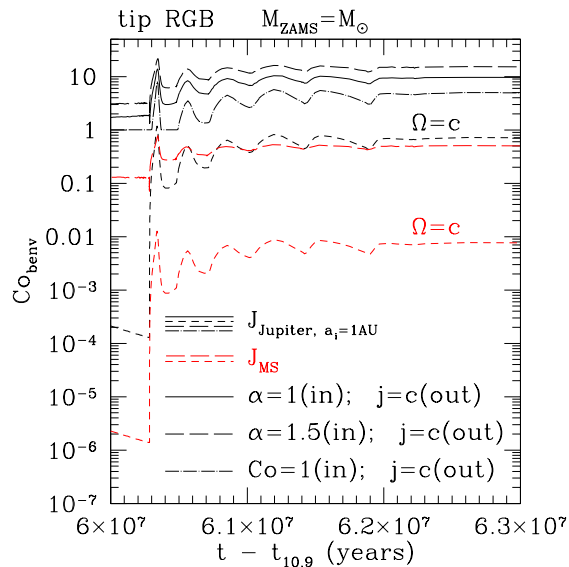
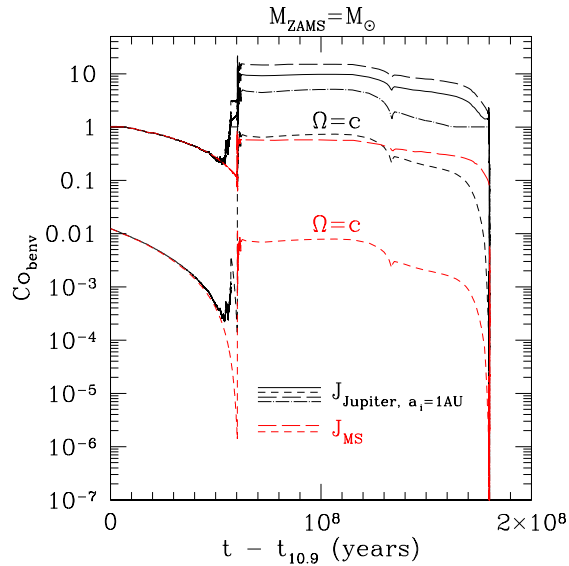


FIG. 10.— Evolution of the Coriolis parameter at the base of the convective envelope. Curves correspond to those in Figure 9. Upper panel shows the RGB, core helium burning phase, and AGB. Lower panel shows an expanded view of the tip of the RGB and the beginning of the core He burning phase.

we obtain

$$\Omega_{\text{benv}} = \frac{J_{\star}}{I_{\text{eff}} + I_{\text{core}}}. \quad (18)$$

Excepting near the point where the envelope has been ejected at the end of the AGB, the moment of inertia of the core can generally be neglected,  $I_{\text{core}} \ll I_{\text{eff}}$ .

The angular momentum stored in the core is enhanced by a factor  $\sim (R_{\star}/R_{\text{benv}})^2$ , as compared with the case of solid rotation throughout the star. This simple rotation model breaks down when it predicts  $\text{Co} \gtrsim 1$  at the base of the convective envelope, and we employ the modified rotation profiles (9), (10).

Considering first the  $1 M_{\odot}$  model, we compare several scenarios. The star is either assumed to evolve in isolation; or to interact with a Jupiter-mass planet that starts in a circular orbit of semi-major axis 1 AU. The internal

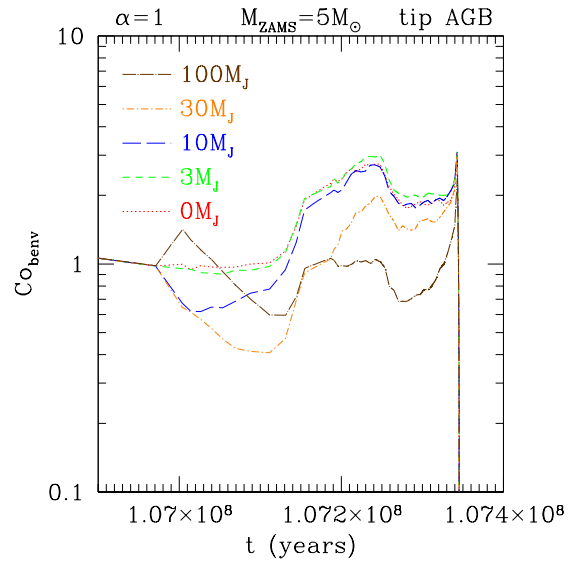
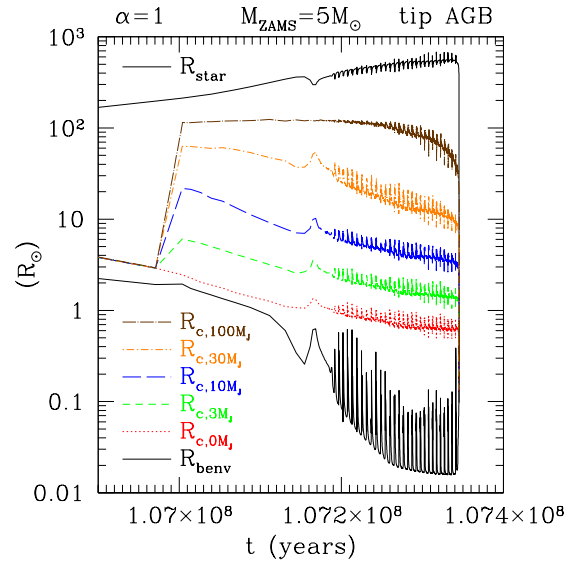


FIG. 11.— Effect on the  $5M_{\odot}$  model star of the engulfment of a substellar companion of mass  $(3, 10, 30, 100)M_{\text{Jupiter}}$  from an initial orbit  $a_i = 2$  AU. Orbital angular momentum of planet is added to star when it reaches a radius  $R_{\star} = 200R_{\odot}$  on the AGB, as guided by more detailed tidal evolution calculations. The physical consequences depend weakly on the epoch of engulfment, if it occurs before the first thermal pulse (at  $t \sim 1.0717 \times 10^8$  years), when the envelope dynamo begins to contribute to the magnetic field of the hydrogen-depleted core. Upper panel: time evolution of transition radius  $R_c$  between outer slowly rotating zone ( $\text{Co} < 1$ ) and inner rapidly rotating zone ( $\text{Co} > 1$ ). Bottom panel: change in  $\text{Co}_{\text{benv}}$  due to the added angular momentum. Rotation profile corresponds to  $\alpha = 1$  in Equation (9). Although  $R_c$  increases with increasing angular momentum,  $\text{Co}_{\text{benv}}$  decreases.

rotation profile is either described by a two-layer model (Section 4.2) during its post-MS evolution ( $j = c'$  in the outer envelope, with various inner  $\Omega(r)$  profiles); or it is assumed to be solid-body from the ZAMS to the terminal AGB ( $\Omega = c'$ ).

Figure 9 shows the evolution of  $J_{\star}$ . We see that solid-body rotation leads to a significant loss of angular momentum through the RGB winds, because little angular momentum is stored deep in the star. Introducing an

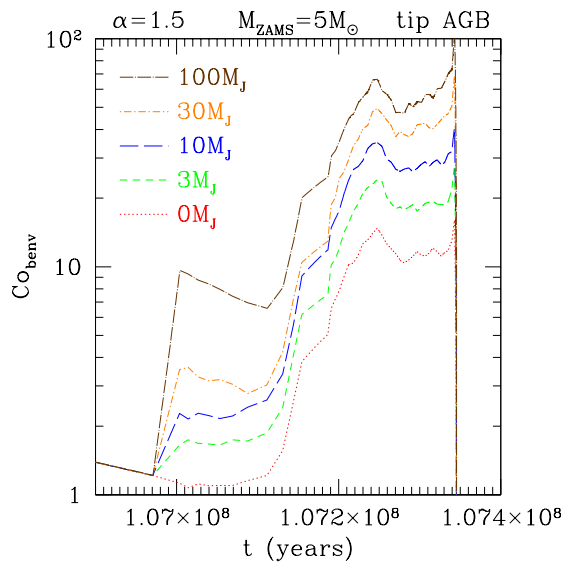


FIG. 12.— Same as bottom panel of Figure 11, but now with steeper inner rotation profile  $\alpha = 1.5$  in Equation (9). Now  $\text{Co}_{\text{benv}}$  increases monotonically with the added angular momentum.

outer zone of uniform specific angular momentum allows only 1/2 of the angular momentum present at the end of the MS to be lost, with the remainder retained at the onset of core He burning. The engulfment of the Jupiter greatly augments  $J_*$ , but if  $\Omega$  is uniform then most of this additional angular momentum is lost to RGB winds.

The most important consideration for us is whether  $\text{Co}_{\text{benv}}$  reaches the threshold for dynamo activity. The time dependence of  $\text{Co}_{\text{benv}}$  is shown in Figure 10. Only in the case of planet absorption with ‘ $j = c$ ’ in the outer envelope does the star comfortably pass this threshold. Enough angular momentum is absorbed from a Jupiter-mass planet that almost any profile  $\Omega(r) \propto r^{-\alpha}$  with  $\alpha > 0$  will allow the star to attain  $\text{Co}_{\text{benv}} = 1$  on the RGB. Stronger angular momentum pumping is required near the tip of the AGB to sustain rapid rotation: uniform rotation combined with absorption of a Jupiter does not suffice.

An isolated  $M_{\text{ZAMS}} = 1 M_{\odot}$  star without a planetary companion does not attain  $\text{Co}_{\text{benv}} \sim 1$  in its inner envelope near the tip of the RGB or AGB, no matter the rotation profile. This dynamo threshold is missed by more than two orders of magnitude in the case of solid rotation.

Angular momentum could also be transferred to an evolved giant by a tidal interaction with a stellar companion. This happens inevitably during the evolution to a common envelope and the formation of pre-CV system. For example, the  $5M_{\odot}$  star may easily engulf a companion during the AGB phase, given the large maximum radius reached by the star ( $\sim 600R_{\odot}$ ). We consider the effect of injecting a companion of mass  $(3, 10, 30, 100)M_{\text{Jupiter}}$  from an orbit with initial semi-major axis  $a_i = 2\text{AU}$  when the star reaches a radius  $R_{\star} = 200R_{\odot}$  on the AGB. We also consider a range of inner rotation profiles,  $\alpha = 1$  to 1.5 in Equation (9).

Figure 11 shows that the added angular momentum pushes  $R_c$  outward, as expected; but when  $\alpha = 1$  the relative flatness of the  $\tau_{\text{con}}(r)$  profile ( $\tau_{\text{con}}$  increasing

roughly in proportion to  $r$ ) may actually cause  $\text{Co}_{\text{benv}}$  to decrease. In other words, the engulfment of a more massive companion may result in slower rotation at the base of the convective envelope. Increasing the rotation index to  $\alpha = 1.5$  allows  $\text{Co}_{\text{benv}}$  to grow with increasing injected angular momentum (Figure 12). Our inference that angular momentum pumping in the envelopes of subgiants can sustain  $\text{Co}_{\text{benv}} \sim 10$  (see Figure 3) suggests that the rotation profile in the inner envelope may be significantly steeper than  $\alpha = 1$  near the tip of the RGB and AGB. This would imply an even stronger magnetization of the WD remnant, as we show in Paper II.

## 5. ORBITAL EVOLUTION OF A PLANETARY COMPANION TO A $1M_{\odot}$ STAR

Our calculation of the interaction of a planet with an evolving giant star follows the orbit in some detail. We take into account the dissipation of the tide raised on the star, and gravitational scattering off a fluctuating quadrupole moment. The second effect, which has been previously considered in the context of massive neutron star binaries (Phinney 1992), has a weaker radial dependence than the tidal torque and therefore modestly increases the range of semi-major axis over which a strong interaction between planet and star can take place.

We evolve the planet’s orbit in response to these external forces, considering a range of masses (Earth, Neptune or Jupiter) along with different initial semi-major axes ( $a_i = 0.5, 0.75, 1, 1.5, 2 \text{AU}$ ) and eccentricities ( $e_i = 0, 0.1, 0.5$ ). The change in orbital angular momentum is deposited in the star and tracked self-consistently, including the effect of stellar mass loss described by Equation (13).

The tidal acceleration is calculated using (Hut 1981)

$$\frac{d^2\mathbf{r}}{dt^2} = -3k_2 \frac{GM_p}{r^2} \left(\frac{R_{\star}}{r}\right)^5 \left[ \left(1 + 3\frac{\dot{r}}{r}\tau\right)\hat{r} - (\Omega_{\text{env}} - \omega)\tau\hat{\phi} \right]. \quad (19)$$

In the above expression, the position of the planet is followed in spherical coordinates, with  $\omega$  its orbital angular velocity and  $M_p$  its mass. We set the rotation frequency  $\Omega_{\text{env}}$  of the stellar envelope<sup>1</sup> to zero. The time lag of the tidal bulge is given by

$$\tau \sim 2 \frac{R_{\star}^3}{GM_{\star}\tau_{\text{con}}} \quad (20)$$

where

$$\tau_{\text{con}} \sim \left(\frac{M_{\text{env}}R_{\star}^2}{L_{\star}}\right)^{1/3} \quad (21)$$

is the global convective overturn time. The Love number  $k_2$  is obtained (see Equations (11) of Zahn 1989 and (17) of Scharlemann 1982),

$$k_2 = 20.5\alpha^{4/3} \frac{R_{\star}^{1/3}\tau_{\text{con}}}{M_{\text{env}}} \int_{x_{\text{benv}}}^1 x^{22/3} L_r^{1/3} \rho^{2/3} l_P dx. \quad (22)$$

Here  $\alpha = 2$  is the convective mixing length parameter,  $M_{\text{env}} = M_{\star} - M_{\text{benv}}$  is the mass of the convective envelope of the star,  $x = r/R_{\star}$ ,  $x_{\text{benv}} = R_{\text{benv}}/R_{\star}$ , and  $L_r$  is the luminosity at a given radius.

<sup>1</sup> Equation (19) is derived assuming solid rotation in the envelope.

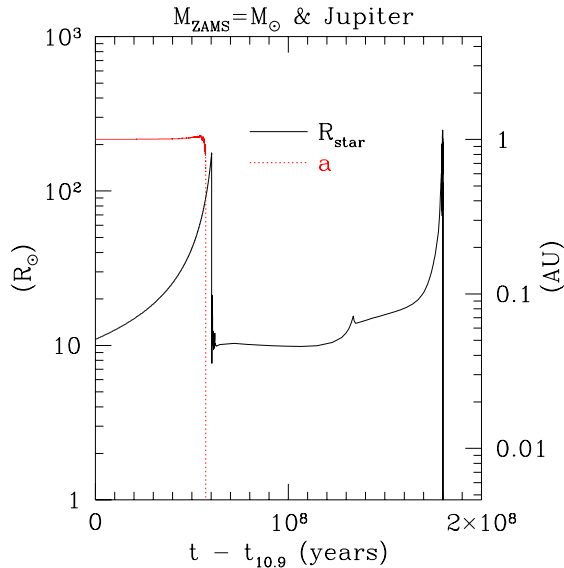


FIG. 13.— Red line: orbital semi-major axis of a Jupiter-mass planet interacting with a RGB star and starting from a circular orbit with  $a_i = 1$  AU. Black line: stellar radius. Spiral-in of planet just below the tip of the RGB deposits angular momentum and triggers a dynamo process near the core-envelope boundary (Paper II).

The acceleration from the convective quadrupole is calculated using the standard expansion of the gravitational potential (see Murray & Dermott 1999),

$$V_{\text{quad}} = -\frac{G}{2r^5} \left[ (I_{yy} + I_{zz} - 2I_{xx})x^2 + (I_{xx} + I_{zz} - 2I_{yy})y^2 + (I_{xx} + I_{yy} - 2I_{zz})z^2 + 6(I_{yz}yz + I_{xz}xz + I_{xy}xy) \right]. \quad (23)$$

(In practice we evolve the orbit of the planet in Cartesian coordinates.) The moment of inertia tensor  $I_{ij}$  is normalized using the rms convective quadrupole

$$\frac{Q_{\text{con}}}{M_{\text{env}}R_{\star}^2} \simeq 7.41 \times 10^{-3} f \frac{L_{\star}^{2/3} R_{\star}^{5/3}}{(M_{\star}/M_{\odot})(M_{\text{env}}/M_{\odot})^{2/3}}. \quad (24)$$

Here  $f$  is a factor of order unity which depends on the stellar structure. This expression is obtained by integrating the density perturbation caused by convection inside the star over the envelope; see the Appendix A for a derivation.

At time intervals separated by  $\tau_{\text{con}}$ , the diagonal components of the moment of inertia matrix for the quadrupole were chosen randomly, with a magnitude uniformly distributed in the range  $[0, Q_{\text{con}}]$ . The remaining components were then obtained by a random rotation of the diagonal matrix. Given the random nature of this forcing effect, we ran ten realizations for each set of initial conditions to obtain a statistical sample of results.

A planet that is exposed to the tidal acceleration (19) and quadrupolar potential (23) will evolve in semi-major axis and eccentricity. It can either collide with the envelope of the star or be ejected from the system. Here we are interested primarily in initial conditions leading to a collision. In such an instance, we assume that drag and dynamical friction act instantaneously, resulting in

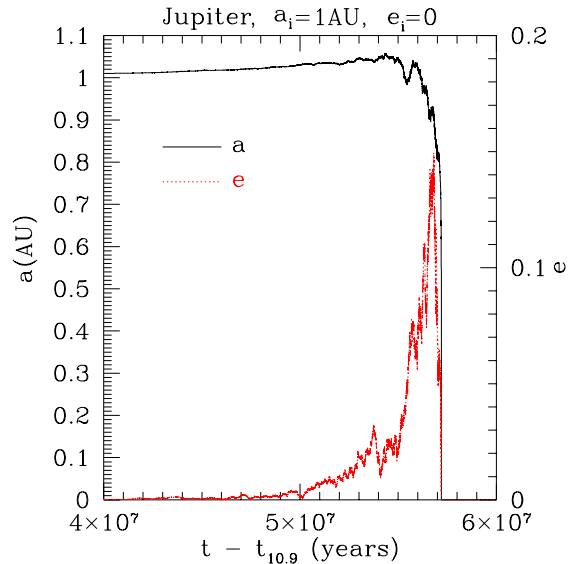


FIG. 14.— Expanded view of the orbital parameters of the Jupiter-mass planet in the same realization shown in Figure 13. Engulfment of the planet is preceded by a stochastic growth in orbital eccentricity, due to gravitational scattering off the convective quadrupole.

the planet's engulfment and the transfer of its orbital angular momentum to the giant.

### 5.1. Jupiter-mass Planet with $a_i = 1$ AU

Consider a Jupiter-mass planet starting at  $a_i = 1$  AU and  $e_i = 0$ . In Figure 13 we show one realization of its orbital evolution, comparing semi-major axis  $a$  with  $R_{\star}$ . In this case the planet is engulfed shortly before the star reaches the tip of the RGB. We treat this as our fiducial model for a  $M_{\text{ZAMS}} = 1 M_{\odot}$  star interacting with a planet.

The corresponding eccentricity evolution is shown in Figure 14. The stochastic nature of the convective forcing of orbital parameters is evident here.

### 5.2. Other Planetary Configurations

Figure 15 shows the probability of a planet's engulfment as a function of the initial (specific) orbital angular momentum. Results for the three planetary masses we consider are shown separately. The separate effect of shutting off the convective quadrupole ( $Q_{\text{con}} \rightarrow 0$ ) is also shown.

The convective forcing has an especially strong effect on the probability of engulfment for Earth-mass planets. In the case of a Jupiter-mass planet, there is a  $\sim 20\%$  enhancement in the range of semi-major axes that results in a merger. These effects arise mainly from the excitation of eccentricity and a corresponding reduction in periastron.

## 6. CONCLUSIONS

We have considered the inward pumping of angular momentum in a deep stellar convective envelope, with a goal of defining a workable rotation model for giant stars. Independent theoretical and observational lines of argument point to a profile that differs radically from those obtained from stellar evolution codes such as MESA, in

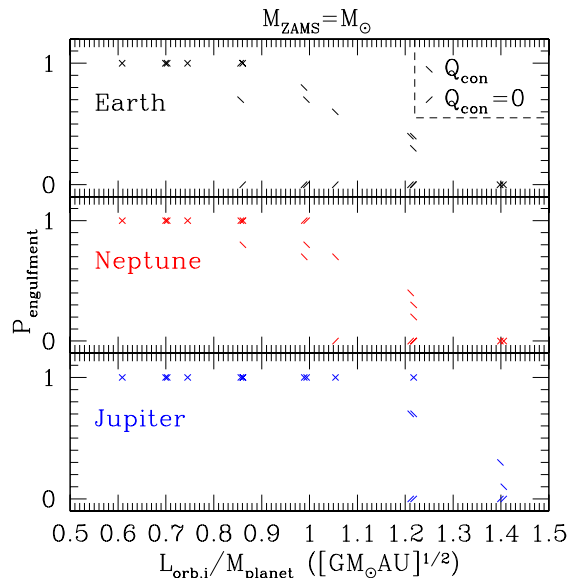


FIG. 15.— Probability of engulfment of planets of various masses (Earth, Neptune, Jupiter), as a function of the initial specific orbital angular momentum. Negative-sloping dash: planet scatters gravitationally off convective quadrupole of giant star. Positive-sloping dash:  $Q_{\text{con}} = 0$ . Probability of engulfment is enhanced by interaction with the quadrupole, especially for lower-mass planets.

which the implementation of angular momentum transport typically results in solid rotation within convective layers. The work presented here and in Paper II also demonstrates that much improved dynamo models must be implemented in order to capture basic features of stellar rotation, such as the relaxation to solid rotation in radiative parts of a star, and the rotational coupling between a radiative core and the base of an extended convective envelope.

The rotation of evolving stars cannot be understood even in qualitative terms without including the magnetic field built up by a hydromagnetic dynamo operating near the boundary between convective and radiative zones. Some features of this dynamo are special to giant stars. First, the high radiative energy flux leads to a strong broadening of the tachocline layer situated beneath the core-envelope boundary, which may facilitate mixing of core material into the envelope. The growth of the core is also accompanied by an inward flux of magnetic helicity. These effects are investigated in detail in Paper II, where we motivate a strong magnetic coupling between core and inner envelope when  $\text{Co}_{\text{benv}} \gtrsim 0.1 - 0.3$ .

When this condition is satisfied, a simple picture emerges: nearly solid rotation in the radiative parts of the star that previously supported a dynamo, combined with an inhomogeneous rotation profile in a deep convective envelope, whose slope depends on the local Coriolis parameter. For example, solid rotation in a radiative layer adjacent to convective zone is facilitated by a tiny helical magnetic field. Differential rotation that is sourced by a changing stellar mass profile during subgiant expansion can be significantly reduced if the poloidal magnetic pressure exceeds  $\sim 10^{-16} - 10^{-15}$  of the convective pressure, increasing to  $\sim 10^{-8}$  during the thermally pulsating AGB. Magnetic fields  $\sim 10^2 - 10^3$  times stronger are required to compensate a latitude-

dependent convective stress that is partly transmitted through a tachocline layer (Paper II).

A magnetic field exceeding this minimal value is plausibly present in the radiative core of a subgiant: erasure to a lower level would require a very efficient mechanism for eliminating magnetic helicity. Inhomogeneous rotation could, in principle, be maintained by a supplementary mechanism of angular momentum transport such as gravity wave damping.

Our results can be summarized as follows.

1. Strong inward pumping of angular momentum is well motivated by measurements of core rotation in stars of radius  $\lesssim 10 R_{\odot}$  (Beck et al. 2012; Mosser et al. 2012), and by numerical simulation (Brun & Palacios 2009). A rotational decoupling between core and envelope (as envisaged e.g. by Cantiello et al. 2014) is difficult to achieve over the long duration of subgiant expansion, depending on an unrealistically small poloidal magnetic field. We have found that a profile  $\Omega(r) \propto r^{-1}$  within parts of the envelope that are very rapidly rotating ( $\text{Co} \gtrsim 1$ ), combined with solid rotation in the radiative core, provides an excellent fit to the data for stars more massive than  $\sim 1.3 M_{\odot}$ . This corresponds to the profile that is derived from quasi-geostrophic balance in an adiabatic envelope with heat transported by radially extended convective upflows and downflows that do not mix significantly with each other over a scale height. Given a gravity profile  $g(r) \propto r^{-\beta}$  with  $\beta \simeq 1$ , we deduce  $\Omega(r) \propto r^{-(1+\beta)/2} = r^{-1}$ .

More focused measurements of individual stars can in principle be used to test this rotation model – in particular, to constrain the range of  $\Omega$  within the convective envelope – and also to test for the existence of strong differential rotation across the core-envelope boundary, as in the model of Cantiello et al. (2014). Efforts so far to measure the full radial profile  $\bar{\Omega}(r)$  have considered separate zones of solid rotation in core and envelope, as well as smoother profiles; the fits are mainly sensitive to the rotation rate in the core (Deheuvels et al. 2012, 2014).

Solar-mass stars which spin down significantly on the MS, and do not absorb a planetary companion, are predicted to retain much slower core rotation during subgiant expansion, but to rotate within the range of rates inferred from *Kepler* observations of core He burning stars. Although the *Kepler* subgiant sample is mainly composed of stars more massive than  $1.3 M_{\odot}$ , this provides a sharp test of the rotation model presented here. On the other hand, we note that convergence in the core rotation of stars below and above the  $1.3 M_{\odot}$  threshold during subgiant expansion would be remarkable in almost any rotation model, given the significant difference in rotation rate at the end of the MS.

2. Independent constraints on internal rotation in subgiants come from measurements of the slowdown in surface rotation as stars of mass  $\gtrsim 1.3 M_{\odot}$  first ascend the giant branch. A good part of the discrepancy, found by Schrijver & Pols (1993), with stellar models which assume solid rotation, is removed by introducing the same envelope rotation profile that is implied by the *Kepler* asteroseismic data. A separate rapidly rotating core, combined with solid rotation in the envelope, has a negligible effect on surface rotation because  $I_{\text{core}}$  is a very small fraction of  $M_{\text{benv}} R_{\text{benv}}^2$  (and of the effective moment of

inertia of the envelope).

3. Stars near the tip of the RGB and AGB (radii  $\gtrsim 10^2 R_\odot$ ) probe a different regime of slow rotation that is not directly constrained by the *Kepler* observations. Here we have considered steeper rotation profiles,  $j \sim \text{const}$ , in the outer parts of the envelope where  $\text{Co} \lesssim 1$ . This stronger level of angular momentum pumping allows rapid rotation to be sustained deep in the envelope even during the final stages of envelope ejection. It also limits the loss of angular momentum to winds on the RGB and AGB. We find that the conditions for a hydro-magnetic dynamo are favorable in a star which rotates rapidly at the end of the MS (e.g. initial mass  $\gtrsim 1.3 M_\odot$ ); or in a solar-mass star which absorbs a Jupiter (or even Neptune) at some point during its post-MS expansion.

The gravity profile steepens significantly in the inner envelope following the first dredge-up phase, and approaches  $g(r) \propto r^{-2}$  near the tips of the RGB and AGB. If the convective upflows and downflows remain radially extended, then our scaling solution to the vorticity equation implies that the inner angular velocity profile steepens to  $\Omega(r) \propto r^{-3/2}$ .

4. The mass of an individual convective cell in a giant envelope greatly exceeds the mass of Jupiter. This means that the orbital eccentricity of any planet will be significantly excited by the associated gravitational quadrupole. We have calculated the orbital evolution of a suit of planets of various masses (Earth, Neptune, Jupiter) in response to this gravitational stirring as well as tidal drag. The gravitational stirring has a significant effect on the probability of absorption of an Earth-mass planet starting at a semi-major axis 1 AU.

5. The case of a solar-mass star which spins down on the MS and then *does not* regain angular momentum from a companion is more complicated. The rotation model described here can be applied while the star remains more compact than  $R_\star \sim 10^{12}$  cm; but slow rotation is encountered throughout the convective envelope near the tip of the giant branches. In these most extended phases of expansion, the coupling between core and envelope will depend on additional (and perhaps largely hydrodynamic) mixing mechanisms, whose exact nature is still being debated (Maeder & Meynet 2000; Fuller et al. 2014).

More extended simulations of deep convection, including radiative transport and feedback from magnetic fields, are required to confirm the dependence of rotation profile on Coriolis parameter. A more centrally peaked profile is plausibly achieved near maximum expansion on the giant branches, where the effects of rotation are weaker, but whether this profile really approaches uniform specific angular momentum needs further testing. We emphasize the degeneracy between the combined effects of flattening the slope of the rotation profile and increasing the spindown on the MS (both of which reduce the rotation rate in the inner envelope), and raising the angular momentum that is received from a sub-stellar companion during post-MS expansion. Although magnetic field amplification in the inner envelope becomes more difficult as the rotation profile flattens, even a planetary companion can have a significant compensating effect.

This work was supported by NSERC. We thank the anonymous referee for detailed comments on the presentation of our results.

## APPENDIX

### NORMALIZATION OF CONVECTIVE QUADRUPOLE DURING GIANT EVOLUTION

The internal density, temperature and luminosity profiles of a model giant star evolve with time in a complicated way. Here we describe a simple prescription for the net gravitational quadrupole that is induced by convective motions in the giant envelope, which can be expressed in terms of integral quantities such as stellar luminosity  $L_\star$ , radius  $R_\star$  and core and envelope masses  $M_{\text{core}}$ ,  $M_{\text{env}}$ .

We estimate the magnitude of the quadrupole from

$$Q_{\text{con}} \simeq \sqrt{N_{\text{cells}}} \langle \delta M r^2 \rangle \quad (\text{A1})$$

where  $N_{\text{cells}}$  is the number of convective cells in the envelope of the star, and  $\delta M$  is the mass perturbation induced by convection in a cell, and the average is over the volume of the envelope. We assume that the convective cells (of angular size  $\Delta\Omega$ ) penetrate the whole star, so that

$$N_{\text{cells}} \sim \frac{4\pi}{\Delta\Omega}; \quad \langle \delta M r^2 \rangle \sim \Delta\Omega \int_0^{R_\star} r^4 \delta\rho dr. \quad (\text{A2})$$

The density perturbation  $\delta\rho \sim \rho v_{\text{con}}^2 / c_s^2$ , where we estimate  $\rho v_{\text{con}}^3 \simeq L_\star / 4\pi r^2$ . Therefore

$$\langle \delta M r^2 \rangle \sim \Delta\Omega \left( \frac{L_\star}{4\pi} \right)^{2/3} \int_0^{R_\star} r^{8/3} \frac{\rho^{1/3}}{c_s^2} dr, \quad (\text{A3})$$

where we take  $\Delta\Omega = 1$ .

The assumption of a point gravitational potential, in combination with an adiabatic equation of state, gives a good fit to the actual density profile of a giant. The temperature profile is more sensitive to the mass distribution in the star. Hence

$$\rho(r) = \frac{4M_{\text{env}}}{\pi^2 R_\star^3} \left( \frac{R_\star}{r} - 1 \right)^{3/2}; \quad c_s^2(r) = \frac{2}{3} \frac{G}{R_\star} M(<r) \left( \frac{R_\star}{r} - 1 \right) = \frac{2GM_\star}{3R_\star} g \left( \frac{r}{R_\star}, \frac{M_{\text{core}}}{M_\star} \right) \left( \frac{R_\star}{r} - 1 \right), \quad (\text{A4})$$

where  $M(< r)$  is the enclosed mass, which is proportional to

$$g(x, M_{\text{core}}/M_{\star}) = \frac{M_{\text{core}}}{M_{\star}} + \frac{16M_{\text{env}}}{\pi M_{\star}} \int_0^x x'^2 \left( \frac{1}{x'} - 1 \right)^{3/2} dx'. \quad (\text{A5})$$

The quadrupole (A1) works out to

$$\frac{Q_{\text{con}}}{M_{\text{env}} R_{\star}^2} \simeq \frac{3}{4^{1/3} \pi^{5/6} G} \frac{\Delta \Omega^{1/2} L_{\star}^{2/3} R_{\star}^{5/3}}{M_{\text{env}}^{2/3} M_{\star}} f; \quad f \equiv \int_0^1 \frac{x^{8/3}}{g(x, M_{\text{core}}/M_{\star})} \left( \frac{1}{x} - 1 \right)^{-1/2} dx. \quad (\text{A6})$$

#### REFERENCES

- Balbus, S. A., Hawley, J. F., & Stone, J. M. 1996, *ApJ*, 467, 76  
 Balbus, S. A. 2009, *MNRAS*, 395, 2056  
 Beck, P. G., Montalban, J., Kallinger, T., De Ridder, J., Aerts, C., García, R. A., Hekker, S., Dupret, M.-A., Mosser, B., Eggenberger, P., Stello, D., Elsworth, Y., Frandsen, S., Carrier, F., Hillen, M., Gruberbauer, M., Christensen-Dalsgaard, J., Miglio, A., Valentini, M., Bedding, T. R., Kjeldsen, H., Girouard, F. R., Hall, J. R., & Ibrahim, K. A. 2012, *Nature*, 481, 55  
 Bethe, H. A. 1990, *Reviews of Modern Physics*, 62, 801  
 Blöcker, T. 1995, *A&A*, 297, 727  
 Braithwaite, J. & Spruit, H. C. 2004, *Nature*, 431, 819  
 Browning, M. K., Miesch, M. S., Brun, A. S., & Toomre, J. 2006, *ApJ*, 648, L157  
 Brun, A. S., Miesch, M. S., & Toomre, J. 2004, *ApJ*, 614, 1073  
 Brun, A. S. & Palacios, A. 2009, *ApJ*, 702, 1078  
 Cantiello, M., Mankovich, C., Bildsten, L., Christensen-Dalsgaard, J., & Paxton, B. 2014, *ApJ*, 788, 93  
 Deheuvels, S., García, R. A., Chaplin, W. J., et al. 2012, *ApJ*, 756, 19  
 Deheuvels, S., Doğan, G., Goupil, M. J., et al. 2014, *A&A*, 564, A27  
 Dobbie, P. D., Napiwotzki, R., Burleigh, M. R., Williams, K. A., Sharp, R., Barstow, M. A., Casewell, S. L., & Hubeny, I. 2009, *MNRAS*, 395, 2248  
 Fuller, J., Lecoanet, D., Cantiello, M., & Brown, B. 2014, *ApJ*, 796, 17  
 Gough, D. O. & McIntyre, M. E. 1998, *Nature*, 394, 755  
 Hut, P. 1981, *A&A*, 99, 126  
 Kissin, Y. & Thompson, C. 2015, *ApJ*, in press (arXiv:1501.07197v2)  
 Maeder, A., & Meynet, G. 2000, *ARA&A*, 38, 143  
 Maeder, A., & Meynet, G. 2014, *ApJ*, 793, 123  
 Mosser, B., Goupil, M. J., Belkacem, K., Marques, J. P., Beck, P. G., Bloemen, S., De Ridder, J., Barban, C., Deheuvels, S., Elsworth, Y., Hekker, S., Kallinger, T., Ouazzani, R. M., Pinsonneault, M., Samadi, R., Stello, D., García, R. A., Klaus, T. C., Li, J., Mathur, S., & Morris, R. L. 2012, *A&A*, 548, A10  
 Murray, C. D. & Dermott, S. F. 1999, *Solar System Dynamics* (Cambridge: Cambridge University Press)  
 Paxton, B., Bildsten, L., Dotter, A., Herwig, F., Lesaffre, P., & Timmes, F. 2011, *ApJS*, 192, 3  
 Phinney, E. S. 1992, *Royal Society of London Philosophical Transactions Series A*, 341, 39  
 Reimers, D. 1975, *Memoires of the Societe Royale des Sciences de Liege*, 8, 369  
 Sackmann, I.-J., & Boothroyd, A. I. 1991, *ApJ*, 366, 529  
 Scharlemann, E. T. 1982, *ApJ*, 253, 298  
 Schrijver, C. J., & Pols, O. R. 1993, *A&A*, 278, 51  
 Spruit, H.C. 2002, *A&A*, 381, 923  
 van Saders, J. L., & Pinsonneault, M. H. 2013, *ApJ*, 776, 67  
 Wolf, S. C., Strom, S. E., Dror, D., & Venn, K. 2007, *AJ*, 133, 1092  
 Zahn, J.-P. 1989, *A&A*, 220, 112